

Chapter 1

Integrated Photoluminescence Lifetimes

As OLEDs become fully a fully commercialized technology, several challenges still exist that need to be overcome to realize full potential. Chief among these is the operational lifetime, which has been a key focus of recent studies.^{1–5} Lifetime is typically characterized at constant current density, recording the luminance loss and voltage as a function of time. The lifetime is then reported as the time to reach some arbitrary fraction of the initial luminance. Unlike the steady-state efficiency, it is difficult to optimize a device lifetime by brute force. Due to the long lifetime of devices, even under accelerated aging, it takes a substantial amount of time to characterize devices and iteratively improve a design. This reality makes it essential to have a deeper insight into the processes that are limiting lifetime.

While this simple lifetime characterization is effective for device to device comparison, further insight into the mechanism is found wanting. Modeling techniques are used extensively for degradation characterization, using the mechanisms outlined in Chapter ??.^{6–8} While these techniques are able to reproduce the decay characteristics with a root in physical mechanisms, they suffer from over-parameterization and introduce parameters that cannot be experimentally confirmed. As discussed in Chapter ??, a variety of chemical, structural, and spectroscopic techniques are often employed to gain further insight into the physical processes.^{1,3,4,9,10} These techniques can be insightful, but are difficult to apply on a large scale due to the additional processing time. Post degradation analysis does not provide a temporal characterization of degradation without processing individual devices at several decay points, which can be extremely time consuming. Additionally, it may be helpful to categorize luminance loss into different luminance loss pathways, which few of these techniques are able to do. It would be beneficial to have a technique that is able to provide more information during the degradation, without increasing experimental time, as well as provide a way to decouple loss pathways. This is done by introducing an optical pump to independently measure

η_{PL} as a function of time. Similar techniques have been utilized before, but have lacked completeness in their care to treat assumptions, as well as their resolution.^{11–13}

This chapter demonstrates a method for decoupling the device photoluminescence loss from the exciton formation losses during operational lifetime testing. This is a summary and extension of my work entitled Hershey et al. [14] as well as some error analysis from Bangsund and Hershey [15].

1.1 Luminance as Efficiency Loss

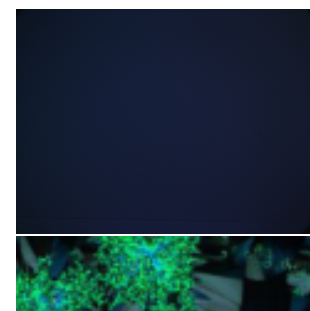
When OLEDs are degraded at constant current density, luminance loss is observed. As discussed in Chapter ??, quantum efficiency is the ratio of photons leaving the device per electron input. Therefore, at constant current density (or constant electron flux), luminance loss is actually an efficiency loss. Chapter ?? extensively discussed a revised formalism for understanding OLED efficiency. In particular, we will take advantage of the formalism of exciton formation efficiency. For decoupling luminance loss pathways, a categorical expression for η_{EQE} is desired, rather than the dynamics approach taken in Equation ??, therefore Equation ?? is modified to include a quenching term, yielding

$$\eta_{EQE} = \eta_{PL} \eta_{OC} \chi \eta_{EF} \eta_\tau \quad (1.1)$$

where η_τ is the fraction of excitons that relax via the natural exciton lifetime, τ . this term is current-density dependent and captures the quenching events discussed in Chapter ???. It is also important to note that during degradation, η_{EF} captures not only the previously discussed polaron loss due to leakage events, but also the formation of non-radiative recombination centers (NRRCs). NRRCs are states that form excitons off of the emissive molecule and allow charge recombination without forming light, which have been shown to be present in degrading devices.^{12,16} The interpretation of η_{EF} as the exciton formation efficiency needs to be clarified to be the efficiency of exciton formation on the emissive molecule, but remains otherwise unchanged.

During degradation, to categorize efficiency loss, each term in Equation 1.1 could be considered to be time dependent. However, it is reasonable to assume that some of these terms are unchanged, or have minimal impact. The exciton's radiative spin fraction, χ is a quantum mechanical property of the emissive molecule. Therefore, without changes in the emissive molecule, this term should remain constant. If emission from another state was observed spectrally, this would indicate a need to adapt Equation 1.1 for multiple emissive states, greatly complicating this process. Thankfully, that is of yet unobserved in our research.

The out-coupling efficiency, η_{OC} , is a property dependent on the layer optical constants and thick-



nesses. Without significant changes in molecular composition and morphology, it is unlikely that η_{OC} should change. The most likely way to create these changes would be through crystallization. This can be investigated by looking at the devices under crossed polarized optical microscopy.¹⁷ Figure 1.1 shows that in our devices, no crystallization is observed. The reference photo, taken from Fielitz *et al.*¹⁷ demonstrates how apparent crystallization would be if present. It is also important to note that η_{OC} depends on the emitter distribution within the device, and thus the recombination zone. If there is a shift in RZ, out-coupling is likely to change. It is difficult to assess recombination zone and unprecedented to measure as a function of degradation. However, this problem is minimized in thin emissive layers, so studies should attempt to focus on thinner EML devices to reduce error.

Lastly, η_τ is assumed to be constant for this work since it cannot be measured quantitatively. An approximation of the impacts of this term are discussed in Section 1.2.4

With these terms assumed to be constant, the only time dependent terms are η_{PL} and η_{EF} , and the time dependent version of Equation 1.1 can be written as

$$\frac{\eta_{\text{EQE}}(t)}{\eta_{\text{EQE}}^0} = \frac{\eta_{\text{PL}}(t)}{\eta_{\text{PL}}^0} \frac{\eta_{\text{EF}}(t)}{\eta_{\text{EF}}^0} \quad (1.2)$$

where X^0 is the initial value of the parameter before degradation. Since $\eta_{\text{EQE}}(t)$ is the luminance loss as a function of time, an independent measurement of η_{PL} would allow a full decoupling of η_{EQE} into η_{PL} and η_{EF} .

1.2 Photoluminescence Characterization

In order to independently measure η_{PL} during degradation, intermittent optical excitation is done using a laser, as shown in Figure fig:schematic. The laser forms a 1mm diameter circular spot on the active device area. The photoluminescence loss observed from this measurement can be related to the photoluminescence efficiency loss by

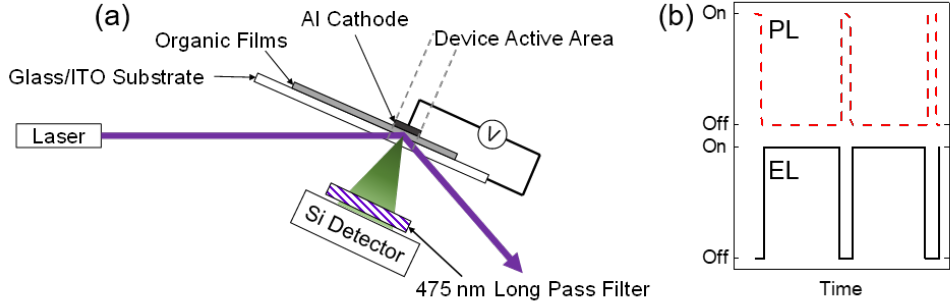


Figure 1.2: (a) Experimental configuration for the measurement of electro- (EL) and photoluminescence (PL) during OLED degradation. Laser excitation is incident on a subsection of the device area. The laser is aligned so that neither the incident nor reflected beam strikes the detector. Stray laser light is removed by a $\lambda=475$ nm dielectric long pass filter. (b) Excitation scheme. EL and PL signals are probed independently with no temporal overlap. (c) External quantum efficiency versus current density and luminance for devices having emissive layer thickness of 10 nm, 20 nm and 30 nm.

$$\frac{\eta_{PL}(t)}{\eta_{PL}^0} = \frac{L_{PL}(t)}{L_{PL}^0} \frac{I^0}{I(t)} \frac{\alpha^0}{\alpha(t)} \quad (1.3)$$

where L_{PL} is the experimentally measured luminance, I is the pump intensity, and α is the film absorption. The pump intensity, I , can be measured and is observed to remain constant within error during the degradation. The absorption, α , has also been measured before and after degradation, and is found to be constant within error. However, the sensitivity of the absorption measurement may not reflect the sensitivity of the η_{PL} measurement. An alternative method to verifying the η_{PL} measurement is presented in Section 1.2.5.

In traditional lifetime measurements, constant current density excitation is used. In order to measure η_{PL} as well, the current is paused every 10 minutes long enough to stabilize the laser and take a measurement, before the current is resumed. This takes on the order of 20 seconds, and is shown in Figure 1.2b. To make these measurements comparable with traditional lifetimes, time is reported as the elapsed time under electrical current, with the laser breaks subtracted. This method has been shown to accurately match the traditional lifetime measurements, without additional degradation due to the PL measurement or relaxation

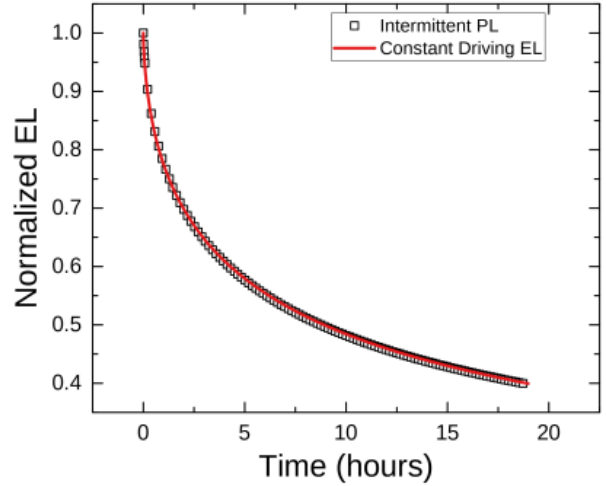


Figure 1.3: Lifetime obtained under a constant driving current is shown in red solid line. Lifetime under the same conditions but with PL measurement breaks is shown in open squares. Strong agreement is observed.

from the breaks in current, as shown in Figure 1.3.

The accuracy of this measurement technique relies heavily on several testing considerations and assumptions. Important considerations of testing conditions and sources of error are discussed in the following sections.

1.2.1 Light Selection

Light sources for optical pumping are required to be powerful enough to pump the emitter sufficiently for measurement, stable enough to maintain output power for lifetimes over 100 hours, and long lived. Ideal candidates are lasers and high power lamps, though lamps often have a long warmup time, which is not ideal for the short on time needed for this experiment. Lamps do have the advantage that they can pump all of the device active area, getting a better sample of the behavior, though lasers can be expanded for the same effect.

During the optical pumping, it is important to only pump the emissive layer, and for the most direct measurement of η_{PL} , only the emitter molecule. To accomplish this, careful selection of wavelength must occur. Figure 1.4 shows the optical extinction coefficient for several materials. Ideally, the pump wavelength should be selected so that the emitter molecule has significant absorption, but the host does not. This is relatively easy for the green emitter, $\text{Ir}(\text{ppy})_3$ where a wide range of pumps would work between 375 and 500 nm. However, This becomes extremely difficult for blue emitters such as $\text{Fir}(\text{pic})$, where hosts are more resonant with the emitter. In this case, the host may have to be pumped and exciton transfer from the host to the guest will be included in the measurement. Even with this, the transport layers would have to have higher triplet energies than the emitter.

Due to these limitations, lasers are ideal light sources for green emitters, since they are easily manipulated optically to pump multiple devices. Here, the limitations of available laser wavelengths are less important due to the wide pumping window. However, for blue emitters, a lamp may be a more viable option as it would allow filtering or monochromation to be more selective of wavelength.

1.2.2 Absorption - Recombination Overlap

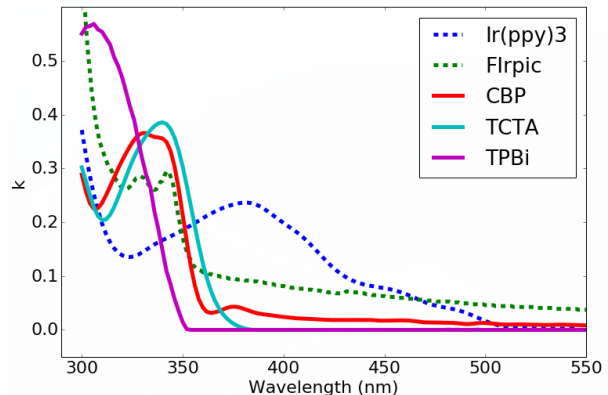


Figure 1.4: Extinction coefficients shown for the green emitter $\text{Ir}(\text{ppy})_3$ and blue emitter $\text{Fir}(\text{pic})$ as well as a few host materials.

Due to these limitations, lasers are ideal light sources for green emitters, since they are easily manipulated optically to pump multiple devices. Here, the limitations of available laser wavelengths are less important due to the wide pumping window. However, for blue emitters, a lamp may be a more viable option as it would allow filtering or monochromation to be more selective of wavelength.

For the measurement of η_{PL} to accurately reflect the useful degradation of the emissive layer, it is important for the optical pump absorption to agree with the recombination zone within the device. To illustrate this, Figure 1.5 shows a device where there is disagreement between the absorption and the recombination zone. Assuming an exciton driven process, defect formation and degradation will focus around the recombination zone. However, optical measurements will probe in the absorption region, which is less degraded than the electrically driven luminance is reflecting. This leads to a systematic underestimate of the actual η_{PL} degradation within the device.

To quantify this error for a particular device, a degradation and defect generation model must be employed in order to quantify the degradation profile within the device. Additionally, the absorption profile and recombination zone must be known (or estimated). The absorption profile can be calculated using a transfer matrix formalism.¹⁸ The code used to calculate this is provided in Appendix ???. The recombination zone can be measured using sensitizer molecules using the method outlined in Chapter ???. An excellent example of executing this analysis demonstrated by Bangsund et al. [19]

1.2.3 Contact Degradation

Exposure to UV light has been shown to enhance photodegradation of the organic/LiF/Al interface within devices.^{9,20} This has been shown to be due to the dissociation and diffusion of positive ions from this interface, likely due to LiF. This becomes problematic in this measurement due to the η_{PL} measurement, as illustrated in Figure 1.6. Here, the optical pump as formed a dark spot on the active area of the device and accelerated degradation.

To minimize this behavior, the laser intensity incident on the device must be kept low. We have found

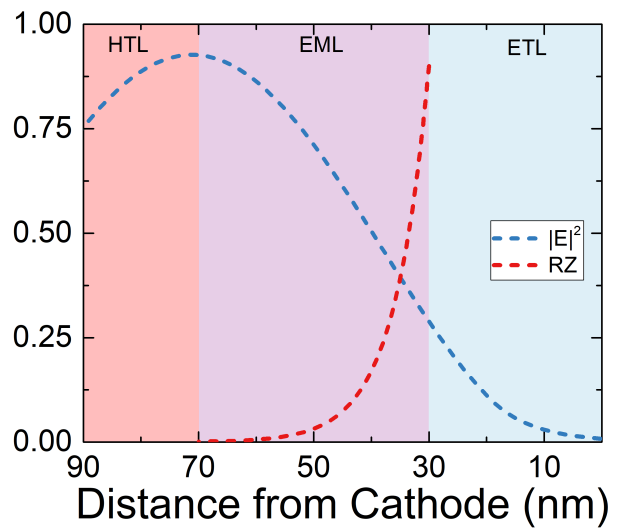


Figure 1.5: Exciton recombination zone (RZ) and pump intensity $|E|^2$ for a hypothetical thick EML device are shown.

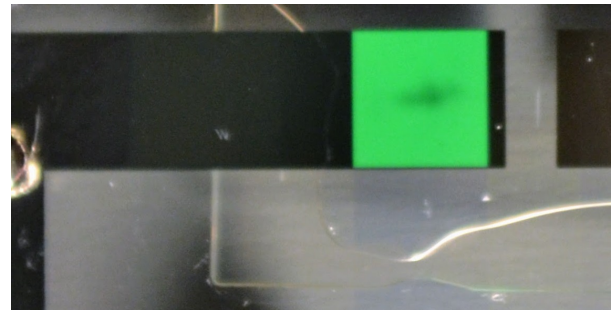


Figure 1.6: Dark spot formation on a device after exposure to a 405 nm laser.

through trial and error that incident powers below 10 mW/cm² for a 405 nm laser do not exhibit this dark spot formation. Devices can be inspected after lifetime testing to ensure that no degradation occurred. We have also observed that for longer wavelengths, the damage power threshold increases and higher power can be used.

1.2.4 Quenching Changes During Degradation

Equation 1.1 introduces a quenching term, η_τ , into η_{EQE} . This term captures bimolecular quenching losses which occur at high current and exciton densities. During lifetime measurements, the exciton density decreases as the efficiency reduces, which will change η_τ . To quantify this, the model presented in Chapter ?? can be used. Using this dynamics formalism, we can define η_τ as

$$\eta_\tau = \frac{1/\tau}{1/\tau + \frac{1}{2}k_{\text{TT}}n_{ex} + k_{\text{TP}}n_{pol}}. \quad (1.4)$$

To find η_τ at the end of degradation, the change in n_{ex} , n_{pol} , and τ must be known. The exciton population, n_{ex} , is known from luminance as discussed in Chapter ?? and the temporal dependence follows the luminance loss assuming the radiative rate remains constant (which we assume). The polaron population likely increases to account for the decrease in our exciton density, but is difficult to quantify. Therefore, for this argument, we will assume it remains constant, though it will likely counteract some of the error that this method will estimate. With the temporal dependence of these quantities known, the time dependence of Equation 1.4 can be written as

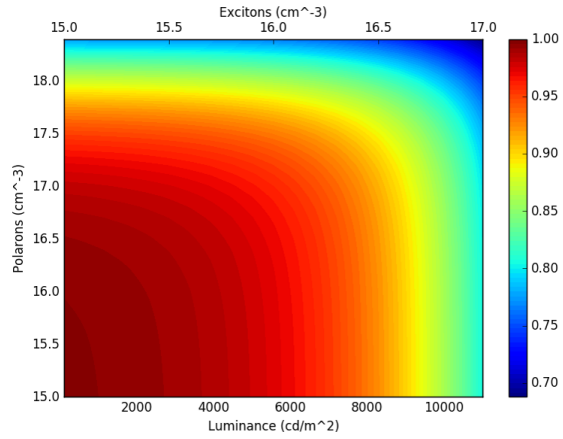


Figure 1.7: Multiplicative correction factor for exciton formation efficiency due to changes in quenching during lifetime. Shown as a function of polaron and exciton density as well as luminance, assuming a 10 nm emissive layer.

$$\frac{\eta_\tau(t)}{\eta_\tau^0} = \frac{1/\tau}{1/\tau + \frac{1}{2}k_{\text{TT}}n_{ex} + k_{\text{TP}}n_{pol}} \frac{1/(R_{PL}(t)\tau) + \frac{1}{2}k_{\text{TT}}(R_{EL}n_{ex}) + k_{\text{TP}}n_{pol}}{1/(R_{PL}(t)\tau)} \quad (1.5)$$

where R_X is the degradation ratio of that term. Since degradation decoupling results are presented assuming $\eta_\tau(t) = C$, the presented out-coupling results can be corrected using $\eta_\tau^0/\eta_\tau(t)$ as a multiplicative correction factor, presented in Figure 1.7. In this figure, minimal correction is needed for low exciton and polaron populations. This only becomes important in regimes where bimolecular quenching are strong. Again, it is important to note that if changes in the polaron population are accounted for, this correction

factor would be further reduced.

1.2.5 Verification with Exciton Lifetime

Alternative to the method for establishing the accuracy of the η_{PL} degradation presented in Equation 1.3, the exciton lifetime can be used. From photophysics, we have

$$\eta_{PL} = \frac{k_r}{k_r + k_{nr}} \quad \tau = \frac{1}{k_r + k_{nr}} \quad (1.6)$$

where k_r and k_{nr} are the radiative and non-radiative decay rates, respectively. From these equations, it is apparent that if k_r remains constant during the degradation,

$$\frac{\tau(t)}{\tau^0} = \frac{\eta_{PL}(t)}{\eta_{PL}^0}$$

Therefore, if the exciton lifetime, τ is measured as a function of decay, it should have a 1-to-1 correlation with the observed PL loss if an accurate measure of η_{PL} is being conducted. To do this, τ is measured from the transient photoluminescence decay at low pump intensity so that minimal triplet-triplet annihilation is observed. This is done on a 337 nm pulsed nitrogen laser, recorded with a fast photodiode connected to an oscilloscope. This has been done for a variety of device architectures, an example of the results being shown in Figure 1.8 for the devices discussed in Chapter ???. Here we see that we are accurately measuring η_{PL} for this device since a strong correlation is observed. The large amount of scatter observed in the 10 nm EML results are believed to be due to the thin EML and small amount of material, producing low signal.

It is important to note for this confirmation of η_{PL} , that this only demonstrates that no absorption or pump intensity deviations are causing error in our measurement. Since the transient photoluminescence and photoluminescence degradation are both pumped optically, both are subject to the recombination zone and absorption mismatch problem discussed in Section 1.2.2.

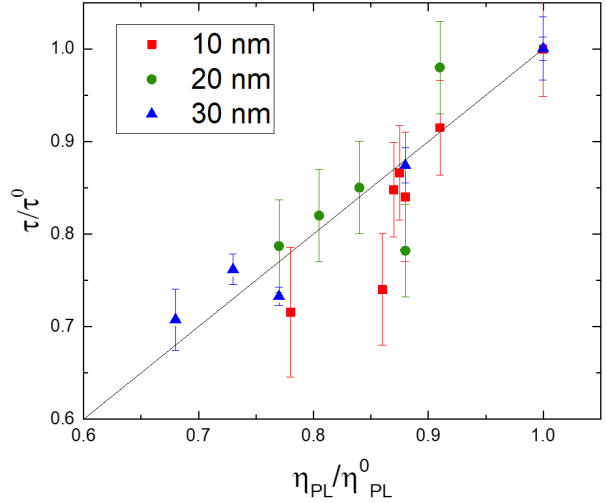


Figure 1.8: Exciton lifetime ratio extracted from transient PL measurements on degraded and undegraded devices as a function of PL degradation for several emissive layer thickness.

1.3 Experimental Implementation

1.3.1 Motivation

The conceptual idea of decoupling η_{EF} and η_{PL} during degradation was first investigated in our group without specialized equipment. Devices were fabricated and aged to varying points in the degradation in the same method as traditional lifetime measurements. After degradation, the device fluorescence was measured using a Photon Technologies International (PTI) fluorometer and compared to a control device. In this way, a PL curve can be produced, shown in Figure 1.9. In this graph, the control is taken as 1 at $t = 0$ and each subsequent point consists of at least one device with three averaged fluorescence measurements for error bars. Though a proof of concept, this method is riddled with experimental problems. First off, experimental throughput is extremely low, since producing any η_{PL} curve requires separate aging of a device for every desired point. Even for the 5 point curves shown, this is extremely equipment heavy. Additionally, every point must be individually measured on the PTI, requiring substantial active lab time from the experimenter, as well as machine time.

The second and more restricting problem with this technique is the large error bars. As shown in Figure 1.9, with error bars of $\pm 10\%$, it is impossible to differentiate between devices. These large error bars for any individual point are caused by differences in loading into the PTI. In this measurement, the raw magnitude of the spectra is being extracted for comparison, and is highly dependent on the exact position of the sample within the excitation beam, as well as alignment with the collection optics and any angular deviation, changing reflection.

Furthermore, this method has no way of eliminating sample-to-sample variation from the η_{PL} curve without reproduction of all experimental points, requiring dramatic increase in machine time. Because of this, only speculation as to the accuracy of the curvature and validity of any data point can be made. Comparison between devices, especially in the temporal behavior becomes impractical due to the experimental time and uncertainty.

These initial experimental techniques demonstrated the need for a new testing method. Ideally, this method would automatically measure η_{PL} on the same sample, dramatically reducing experimental time and throughput limitations. This automatic measurement can have the added benefit of reducing measurement

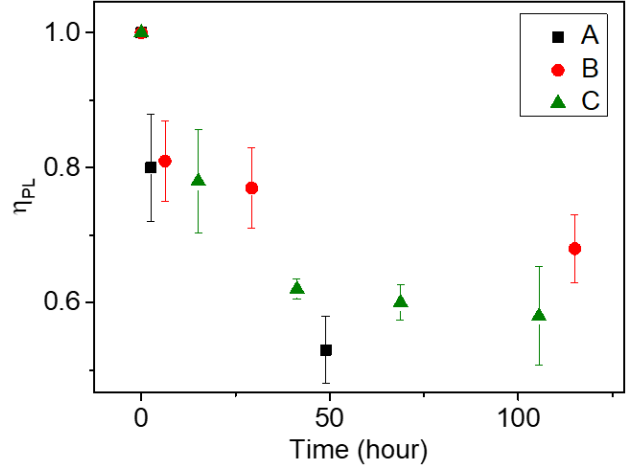


Figure 1.9: Initial Attempts at measuring η_{PL} during degradation using individual devices from the PTI.

The figure shows a scatter plot of η_{PL} versus Time (hour). The x-axis ranges from 0 to 150 hours, and the y-axis ranges from 0.6 to 1.0. Three data series are plotted: Device A (black squares), Device B (red circles), and Device C (green triangles). All three devices show a decrease in η_{PL} over time. Device A shows the most significant decrease, starting at approximately 0.8 at 0 hours and dropping to about 0.55 at 50 hours. Device B starts at approximately 0.8 at 0 hours and drops to about 0.7 at 120 hours. Device C starts at approximately 0.8 at 0 hours and drops to about 0.6 at 100 hours. Error bars are present for all data points.

The second and more restricting problem with this technique is the large error bars. As shown in Figure 1.9, with error bars of $\pm 10\%$, it is impossible to differentiate between devices. These large error bars for any individual point are caused by differences in loading into the PTI. In this measurement, the raw magnitude of the spectra is being extracted for comparison, and is highly dependent on the exact position of the sample within the excitation beam, as well as alignment with the collection optics and any angular deviation, changing reflection.

Furthermore, this method has no way of eliminating sample-to-sample variation from the η_{PL} curve without reproduction of all experimental points, requiring dramatic increase in machine time. Because of this, only speculation as to the accuracy of the curvature and validity of any data point can be made. Comparison between devices, especially in the temporal behavior becomes impractical due to the experimental time and uncertainty.

These initial experimental techniques demonstrated the need for a new testing method. Ideally, this method would automatically measure η_{PL} on the same sample, dramatically reducing experimental time and throughput limitations. This automatic measurement can have the added benefit of reducing measurement

error by holding the sample fixed throughout the decay and ensuring alignment. While sample-to-sample variation may still be an issue, it is no longer a problem in collecting a full dataset.

1.3.2 Development

In order to accomplish this automated measurement, the η_{PL} measurement needed to be conducted in an automated way. A light source capable of producing a constant illumination source over the course of hundreds of hours was needed. A lamp source, such as the PTI was initially considered, but found to have lifetimes similar to the OLED lifetimes. The lamp would not be able to be turned on and off throughout the test since lamps require substantial warmup time to achieve steady-state. Instead, a laser was used since they can be rapidly turned on and off, eliminating any need for blocking the light source during EL measurement. To account for any fluctuations in laser power over time, the power can be measured as a function of time and corrected for if needed.

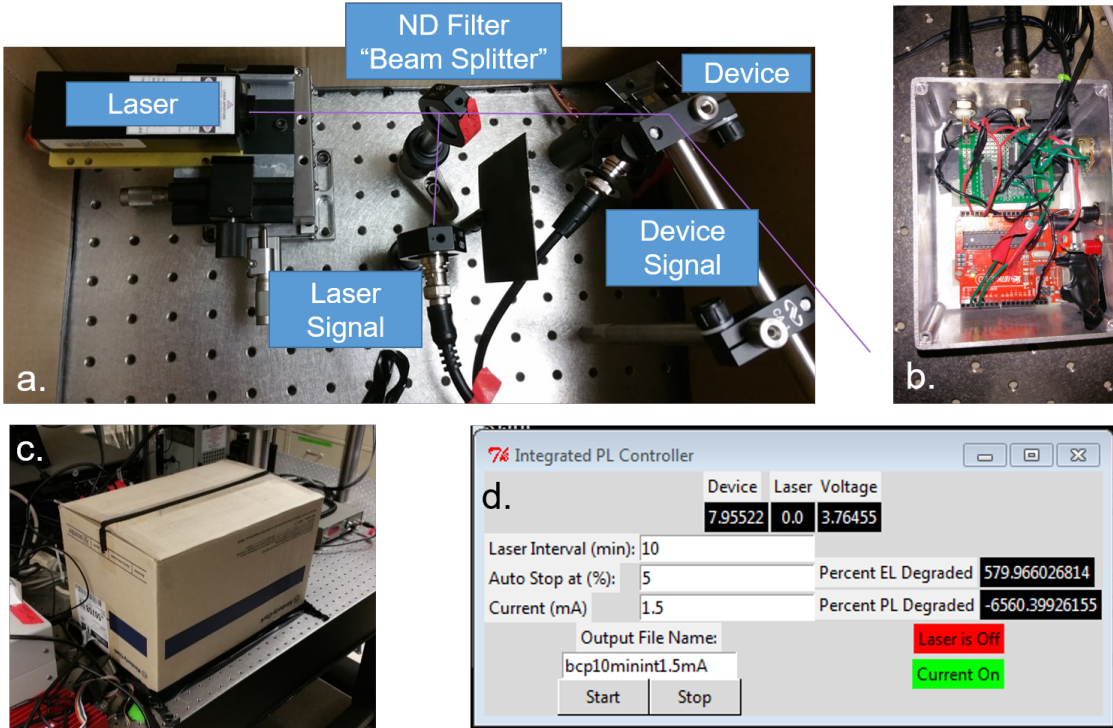


Figure 1.10: First generation lifetime box setup. a. Box layout b. Electronics c. dark enclosure (cardboard box) d. software interface

The first generation implementation of this setup is shown in Figure 1.10. This was a single channel device degradation, with the laser and splitter shown in the Figure 1.10a on the left and the device and photodiode collection shown on the right. Laser power detection relied on the split signal into the photodiode. The electronics are shown in Figure 1.10b and control the laser, current source and voltage measurements, and photodiode measurements. The laser was controlled by switching the interlock using an Arduino (red

PCB). A constant current source was implemented, with the current being set using the potentiometer on the front of the box. This had to be set and measured manually and was only recorded in the software, not set. Photodiode signals were converted to voltages using the green PCB and recorded using the Arduino. The software, shown in Figure 1.10d recorded all measurements and controlled the current, laser, and measurement timings. This was implemented in Python, using the Tk graphics library to create the GUI. At this initial stage, the software only had to interface with the Arduino, and did so using the Serial library. The Arduino was programmed to accept commands to turn on and off the laser and current, or report measurement values for voltage and the signals from either photodiode.

Soon after development, the limited resolution of the photodiode measurements, as well as the limitations of the manual current source were realized. In our traditional measurements of lifetime, a Keithley 26xx source meter was used for sourcing current and measuring signals. This Keithley was rapidly integrated into the system to allow better measurements and more accurate current control. The laser was replaced by a laser from Coherent which offered brighter and more stable power, as well as programmatic control.

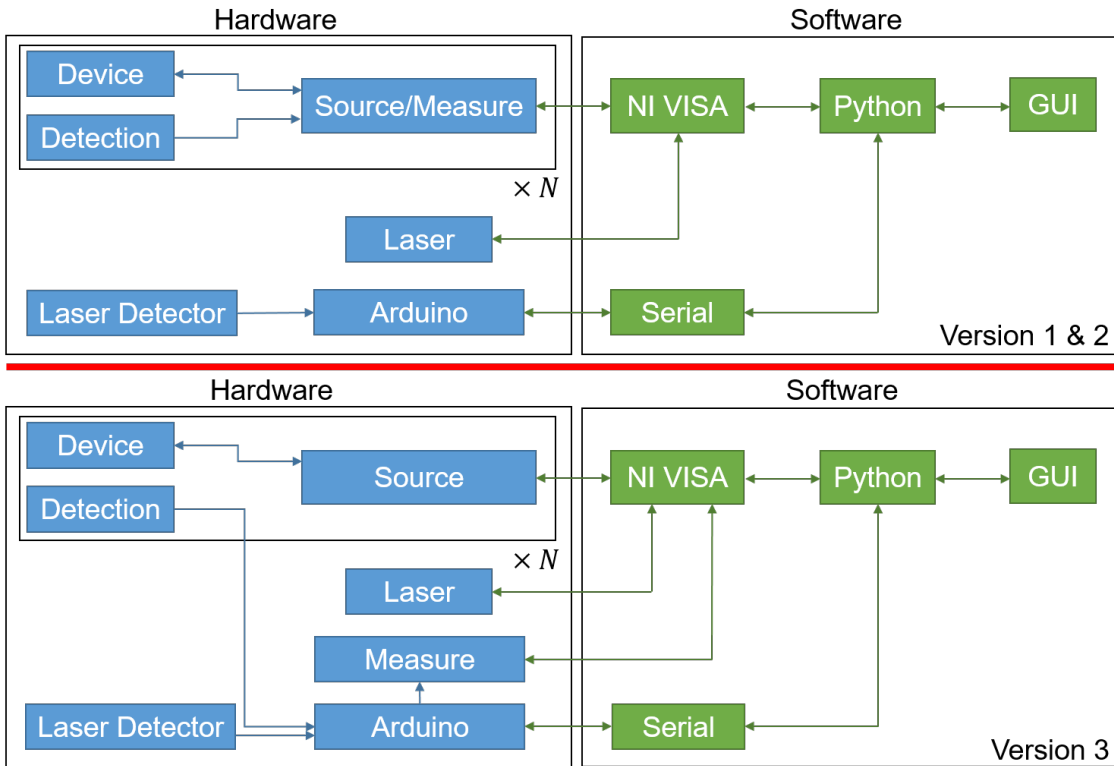


Figure 1.11: Box workflow summary. Top panel shows the operation of Boxes 1 and 2, bottom shows Box 3.

After this early development and hardware changes, little has changed about general workflow of this experiment. However, rather than individual boxes for each experiment, a single laser has been multiplexed to excite up to six different devices, dramatically cutting costs. Each experimental setup consisting of a single laser and multiple testing devices is termed a ‘box’; with each device residing in a compartment. A

summary of all hardware and software connections and control is shown in Figure 1.11. There are two different hardware configurations shown, interfacing with different source-meters. In the top configuration, each compartment is controlled by an individual Keithley source-meter. In the bottom configuration, to cut costs, a Keysight source-meter is used to supply current. The photodiodes in each box are measured by a single Keithley, switching between each compartment using an Arduino relay circuit. This allows a dramatic reduction in hardware and costs.

The next two sections go into detail regarding the implementation of the hardware and software setups.

1.3.3 Hardware Setup

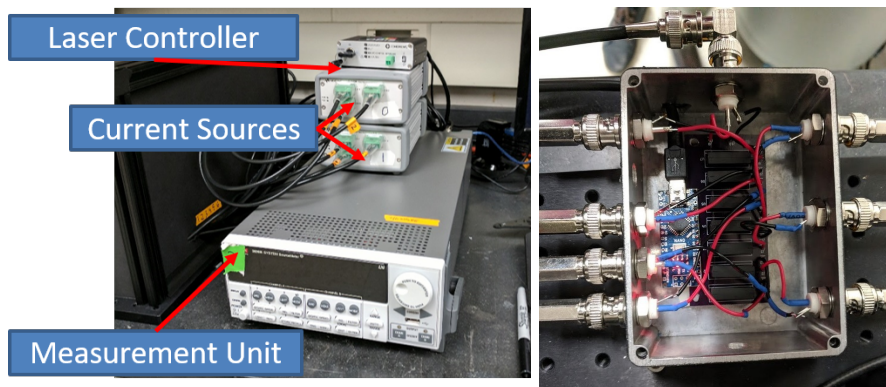


Figure 1.12: Source-Measure hardware and laser controller

Hardware for this setup requires control of current sources, voltage measurement, light source, as well as light measurements. Currently, there are four operational testing setups, termed “boxes”, with varying hardware configurations. Several boxes are multiplexed to allow multiple measurements from the multiple compartments. Source units for providing current and voltage measurements have used either the Keithley 26xx or Keysight u2722a source meters.

The Keithley 26xx units are a two channel, low noise, high precision unit. The Keysight u2722a provides three channels with higher noise and lower precision at a lower price point per channel. Light sources for all boxes are conducted using Coherent OBIS lasers, with wavelengths of either 405 nm or 473 nm. Light measurements are conducted using the Keithley 26xx for all boxes, connected to a Hamamatsu S2281 photodiode. Figure 1.12a shows the electronic hardware setup for a box utilizing

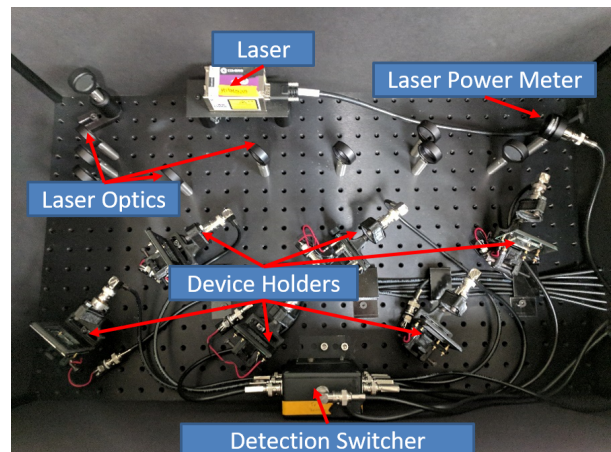


Figure 1.13: Device contacting, measurement, and optical hardware. Version 3 of the hardware is shown. Controlling hardware is shown in Fig. 1.12

Keysights for source units and a Keithley for measurement. To reduce measurement units, the photodiodes in each compartment can be switched between using an Arduino relay system shown in Figure 1.12b. All of these pieces of hardware are compatible with the National Instrument VISA command library for control.

Each device is held by a custom 3D printed vertical mount. The photodiode is wired into this mount with enough space for the laser to avoid the diode. A long pass filter is provided to minimize stray laser signal. The laser is optically split into six paths using beam splitters and neutral density filters are used where necessary to normalize laser power on each device.

1.3.4 Software Development

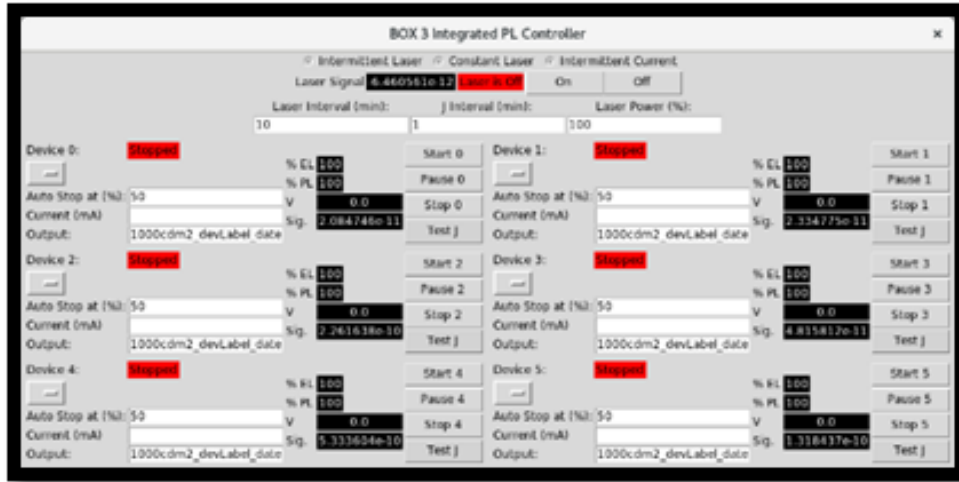


Figure 1.14: 6 channel software controller. Selection of test type, laser control for alignment, and global settings are accessible on the top of the interface. Individual channel settings are grouped on the bottom.

Software to control this measurements is implemented by myself in Python and outlined in Appendix ???. The code is able to control the hardware to run constant current, intermittent laser integrated PL measurements, optical degradation, as well as optical degradation with current break degradations. The frequency of laser breaks and laser power can be controlled on a whole box level. Laser emission can be turned on for alignment. The software is able to be configured to the number of channels available depending on the hardware. Each channel can be individually controlled for current, stop, and labeling.

To organize collected data, a database for all lab data has been developed and is discussed in Chapter ???. Lifetimes integrate with this system when lifetimes are started, using the interface shown in Figure 1.15. Here, a lifetime test is connected to a particular growth, as well as the individual substrate and device pixel. Information about the lifetime is also connected. The lifetime operating current can be determined for a

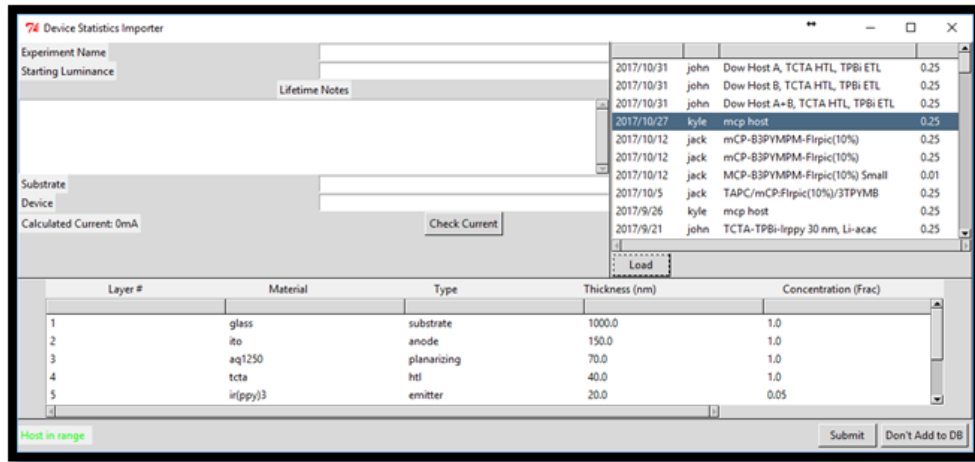


Figure 1.15: Test information for database import interface. The top left panel collects information about the specific device and lifetime. The right panel connects the device to a particular growth and architecture. The bottom panel confirms the architecture.

desired luminance by utilizing the current-voltage-luminance curve for the exact device within this interface.

Additional notes and information are also able to be stored.

1.4 Conclusion

This chapter has outlined a system for decoupling degradation during operational lifetimes. Extensive care has been taken to outline the assumptions and assess error within the extracted parameters. Many of these assumptions need to be assessed for any device system to be tested to ensure accuracy. Applying this method to lifetime decoupling in device systems is the subject of Chapter ??.

Bibliography

- (1) Scholz, S.; Kondakov, D. Y.; Lüssem, B.; Leo, K. *Chemical Reviews* **2015**, *115*, 8449–8503.
- (2) De Moraes, I. R.; Scholz, S.; Lüssem, B.; Leo, K. *Applied Physics Letters* **2011**, *99*, 053302.
- (3) Seifert, R.; Rabelo De Moraes, I.; Scholz, S.; Gather, M. C.; Lüssem, B.; Leo, K. *Organic Electronics: physics, materials, applications* **2013**, *14*, 115–123.
- (4) Moraes, I. R. D.; Scholz, S.; Lüssem, B.; Leo, K. *Organic Electronics* **2011**, *12*, 341–347.
- (5) Burrows, P. E.; Bulovic, V.; Forrest, S.; Sapochak, L. S.; McCarty, D. M.; Thompson, M. E. *Applied Physics Letters* **1994**, *65*, 2922–2924.
- (6) Giebink, N. C.; D’Andrade, B. W.; Weaver, M. S.; MacKenzie, P. B.; Brown, J. J.; Thompson, M. E.; Forrest, S. *Journal of Applied Physics* **2008**, *103*, DOI: 10.1063/1.2884530.
- (7) Ingram, G. L.; Zhao, Y.-B.; Lu, Z.-H. *Journal of Applied Physics* **2017**, *122*, DOI: 10.1063/1.5003011.
- (8) Coburn, C.; Forrest, S. *Physical Review Applied* **2017**, *7*, 041002.
- (9) Wang, Q.; Aziz, H. *Organic Electronics* **2011**, *12*, 1571–1575.
- (10) Zhang, Y.; Aziz, H. *ACS Applied Materials and Interfaces* **2016**, *8*, 14088–14095.
- (11) Popovic, Z. D.; Aziz, H.; Hu, N. X.; Ioannidis, A.; Dos Anjos, P. N. M. *Journal of Applied Physics* **2001**, *89*, 4673–4675.
- (12) Kondakov, D. Y.; Lenhart, W. C.; Nichols, W. F. *Journal of Applied Physics* **2007**, *101*, 024512.
- (13) Winter, S.; Reineke, S.; Walzer, K.; Leo, K. *Proceedings of SPIE* **2008**, *6999*, 69992N–69992N–8.
- (14) Hershey, K. W.; Suddard-Bangsund, J.; Qian, G.; Holmes, R. J. *Applied Physics Letters* **2017**, *111*, 113301.
- (15) Bangsund, J. S.; Hershey, K. W. **2018**.
- (16) Kondakov, D. Y.; Sandifer, J. R.; Tang, C. W.; Young, R. H. *Journal of Applied Physics* **2003**, *93*, 1108–1119.

BIBLIOGRAPHY

- (17) Fielitz, T. R.; Holmes, R. J. *Crystal Growth and Design* **2016**, *16*, 4720–4726.
- (18) Pettersson, L. A. A.; Roman, L. S.; Inganäs, O. *Journal of Applied Physics* **1999**, *86*, 487.
- (19) Bangsund, J. S.; Hershey, K. W.; Holmes, R. J. *ACS Applied Materials & Interfaces* **2018**, acsami.7b16643.
- (20) Wang, Q.; Luo, Y.; Aziz, H. *Applied Physics Letters* **2010**, *97*, 1–4.